Journal of Alloys and Compounds 509 (2011) 5532–5536

Contents lists available at ScienceDirect

Journal of Alloys and Compounds

journal homepage: www.elsevier.com/locate/jallcom

Novel titanium dioxide structure templated from filter paper scales

Jianqiang Li, Qiaoling Li*, Yun Ye, Yan Hao

Department of Chemistry, North University of China, Taiyuan 030051, PR China

ARTICLE INFO

Article history:
Received 16 July 2010
Received in revised form
27 December 2010
Accepted 29 December 2010
Available online 4 January 2011

Keywords:
TiO_2 paper
Microstrip
Filter paper
Template method
Paper-like

ABSTRACT

Titanium dioxide photocatalysts with the interwoven microstrip structure (TiO_2 paper) were successfully synthesized using filter paper as templates. The synthesized samples were characterized by Fourier transform infrared spectroscopy (FT-IR), thermogravimetric analysis (TGA), powder X-ray diffraction (XRD), scanning electron microscopy (SEM) and energy dispersive X-ray fluorescence spectrometer (EDX). The results demonstrated that the samples with the paper-like structure were fully crystallized, and the presence of the filter paper raised the anatase–rutile transformation temperature. Additionally, a detailed formation mechanism for TiO_2 paper is discussed.

© 2011 Elsevier B.V. All rights reserved.

1. Introduction

As the most promising photocatalyst, TiO_2 materials are expected to play an important role in helping treat the polluted water and air because TiO_2 is non-toxic, inexpensive, chemically stable, highly photoactive, and easily synthesized [1,2]. However, TiO_2 photocatalysis is feasible only for the treatment of wastewater that contains contaminants at low to medium pollutant concentrations, because of its relatively low efficiency and the limited flux of ultraviolet photons [3]. Besides, much research has been carried out into a slurry system (suspension of fine powdered TiO_2). The photocatalysts are dispersive, which might pollute the treated water because of the tremendous difficulties in separation and recovery [4]. Using supporting substrates can overcome the separation problem, but the effective surface area of the catalysts will be decreased, which limits the photocatalytic efficiency [5]. Therefore, developing a new type of photocatalyst with high activity and favorable recycling characteristics is a challenge for practical applications. In this regard, various morphological TiO_2 photocatalysts have been found to show some advantages because of their high specific surface area and easiness in operation, recovery and recycling [6,7]. These TiO_2 materials with the special morphology (such as nanotube [8], leaf-like structure [9], nanowire [10] and core–shell structure [6]) have been widely applied in gas sensing [11], solar energy conversion [12], biomedical engineering [13], drug carrier [14], chemical catalysis and photocatalytic [15]. So far, a variety of methods have been used to produce various morphological TiO_2, including electrochemical anodic oxidation [16] and template-based, atomic layer deposition [17] or liquid phase deposition (LPD) method [18]. Particularly, the template-based method is considered to be simple and practical and very attractive. The common template methods have the biological template method [19], the self-template approach [20], and the sacrificial template method [21]. However, reports on filter paper as templates and TiO_2 materials with the paper-like structure (TiO_2 paper) are scanty.

In the present study, the filter paper was applied as the template to successfully synthesize TiO_2 paper photocatalysts with the structure of interwoven microstrips. The presence of the filter paper could improve the crystallinity and raise the anatase–rutile transformation temperature. And the obtained TiO_2 paper could be conveniently affixed to the glass plate with a special paint to recover easily. Furthermore, the waste newspaper can also be utilized to prepare TiO_2 paper.

2. Experimental

2.1. Materials and chemicals

The following chemicals were of analytical grade and were used as received without further purification. Titanium(IV) *n*-butoxide (TBT), hydrochloric acid, and absolute ethanol were purchased from Fuchen Chemical Reagents Factory (China). Titanium dioxide (P25) purchased from Degussa Corporation (Germany) was predominantly anatase (97% anatase and 3% rutile). Filter paper with alkali treatment was immersed in ethanol for 8 h. Deionized water was used to prepare all the solutions.

* Corresponding author. Tel.: +86 351 3923197; fax: +86 351 3922152.
E-mail addresses: li222jianqiang@gmail.com, qiaolingl@126.com (Q. Li).

0925-8388/$ – see front matter © 2011 Elsevier B.V. All rights reserved.
doi:10.1016/j.jallcom.2010.12.193

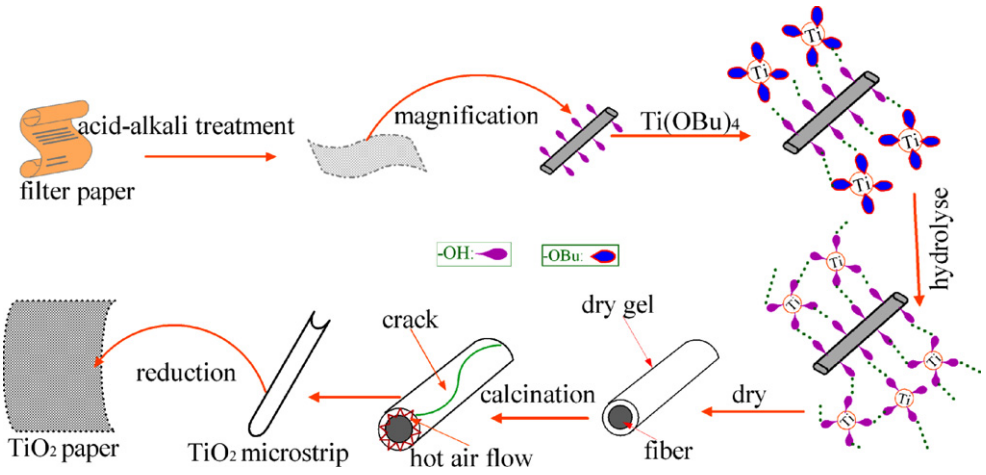

Fig. 1. Representation of the formation of TiO_2 paper composed of microstrips.

2.2. Synthesis of photocatalysts

The TiO_2 paper was prepared by the sol–gel template method. Subsequently, 2 mL aqueous hydrochloric acid (6 M) was added to a solution of TBT (20 mL) and anhydrous ethanol (80 mL) under magnetic stirring, and kept at 30 °C for 30 min. The filter paper was immersed in the resulting solution for 2 h at 30 °C without stirring and treated ultrasonically for 3 h. This was followed by successively filtering, washing in ethanol (2× 10 mL), exposed to the air for 30 min, and then drying at ambient conditions for 3.5 h at 80 °C. The as-synthesized samples (TP_0) were calcined at 500 °C (TP_{500}), 550 °C (TP_{550}), 600 °C (TP_{600}), and 670 °C (TP_{670}) for 2 h, respectively. Subsequently, the TiO_2 paper was obtained.

The TiO_2 powder was prepared as follows: the above filtrated stock was stirred vigorously at 30 °C. After turning into a gel, it was dried at 100 °C. Subsequently, the dry gel was ground and calcined at 600 °C for 2 h to obtain the TiO_2 powder (T_{600}).

2.3. Characterization

Fourier transform infrared (FT-IR) spectra on pellets of the samples mixed with KBr were recorded on a Nexus 670 spectrometer (Nicolet, USA) in the range of 400–4000 cm^{-1} at a resolution of 4 cm^{-1} to identify the chemical structure of the synthesized catalysts. Scanning electron microscopy (SEM) and energy-dispersive X-ray spectroscopy (EDX) were performed on a Hitachi SU-1500 scanning electron microscope to investigate the morphology and elemental analysis of the as-synthesized samples. To determine the phase content and crystallinity of the samples, X-ray diffraction (XRD) patterns were collected on a Rigaku D/Max-ra diffractometer (Cu K_α radiation, $\lambda = 0.15418$ nm, 2θ varied from 20° to 80°) and operated at 40 kV and 200 mA. Further, to determine changes in the weight in relation to changes in the temperature, thermogravimetric analysis (TGA) was performed using a mode 2950 TGA HR instrument with a heating rate of 1 °C/min from 25 to 870 °C under a nitrogen atmosphere.

3. Results and discussion

3.1. Formation of TiO_2 paper

The reaction involving the hydrolysis and condensation between TBT and the hydroxyl groups from the surface of the modified paper fiber as follows: (Eqs. (1)–(3)) [22]:

$$Ti(OBu)_4 + H_2O \rightarrow (BuO)_3Ti\text{–}OH + Butanol \quad (1)$$

$$Ti(OBu)_4 + HO\text{–}Fiber \rightarrow (BuO)_3Ti\text{–}O\text{–}Fiber + Butanol \quad (2)$$

$$(BuO)_3Ti\text{–}OH + HO\text{–}Fiber \rightarrow (BuO)_3Ti\text{–}O\text{–}Fiber + H_2O \quad (3)$$

According to the mechanism of hydrolysis and condensation, the formation pathway of paper-like TiO_2 photocatalyst is shown in Fig. 1. There are abundant hydroxyl groups on the surface of cellulose of the filter paper template. However, the hydrolysis reaction does not occur because of the lack of water when the filter paper is impregnated in a mixture of $Ti(OBu)_4$ and anhydrous ethanol. Thus, there is sufficient time for the formation of the hydrogen bond between $Ti(OBu)_4$ and the hydroxyl groups on the surface of the filter paper. As a result, $Ti(OBu)_4$ absorbed on the fiber surface can easily react with water from the solution or the air to produce $Ti(OH)_4$. This results in the hydrogen bonding formation between $Ti(OH)_4$ and the hydroxyl groups on the filter surface. Simultaneously, $Ti(OH)_4$ molecules are joined to each other by the hydrogen bond. Thereby, the filter paper fibers are coated by the gel. After condensation, a gel layer appears on the fiber surface. In the calcination process of the gel-coated fibers at high temperature, the produced gas flow needs to release and rip should be TiO_2 microtubules to produce the TiO_2 microstrips [23].

The SEM overview of TP_{600} was similar to the texture of the filter paper (not shown), as shown in Fig. 2e. Further, it could be observed that TP_{600} was composed of interwoven TiO_2 microstrips (Fig. 2c). The width and thickness of the microstrip are around 10 μm and less than 1 μm, respectively. The surface of TiO_2 microstrips is rough, which corresponds to the surface morphology of the paper fibers (Fig. 2f). The morphology of TP_{500}, TP_{550} and TP_{600} are similar. But the temperature raises to 670 °C, the crack of the TiO_2 microstrip is apparent (Fig. 2d).

The EDX spectrum in Fig. 3 reveals that the major elements in the TP_{600} paper are titanium and oxygen. Carbon was removed from the solvent and the filter paper in the process of calcination. However, a little nitrogen element was found to exist, which existed in the residues of the filter paper ash.

3.2. FT-IR spectra

FT-IR spectra were applied to identify the chemical structure of synthesized crystals, as well as study the crystal surface chemistry. In Fig. 4a, the sample TP_0 displays a strong and broad composite absorption of 2800–3600 cm^{-1} and 2924 cm^{-1}, wherein the former is associated with the structure or surface hydroxyl groups (including the strongly bound water fibers and titanol [24]) and –OH groups from the adsorbed solvents (ethanol and water), while the latter corresponds to the $-CH_3$ group [25]. The peak at 1632 cm^{-1} relates to the H–O–H bending vibration. However, the intensities of these absorption bands in Fig. 4b–e reduce substantially, thereby indicating that the filter paper template and most of the organic groups have been removed by the pyrolytic calcination. Low-frequency bands in the range of 900–400 cm^{-1} correspond to the Ti–O–Ti vibration of the mineral network, evidencing partial condensation in TP_0 (Fig. 4a). In the spectra of TP_{500}, the intensity of this large band (900–400 cm^{-1}) is enhanced upon thermal treatment. However, the intensities of the bands in Fig. 4b–e show an insignificant improvement with a further increase in the calcination temperature. This implies that the Ti–O–Ti bond is already

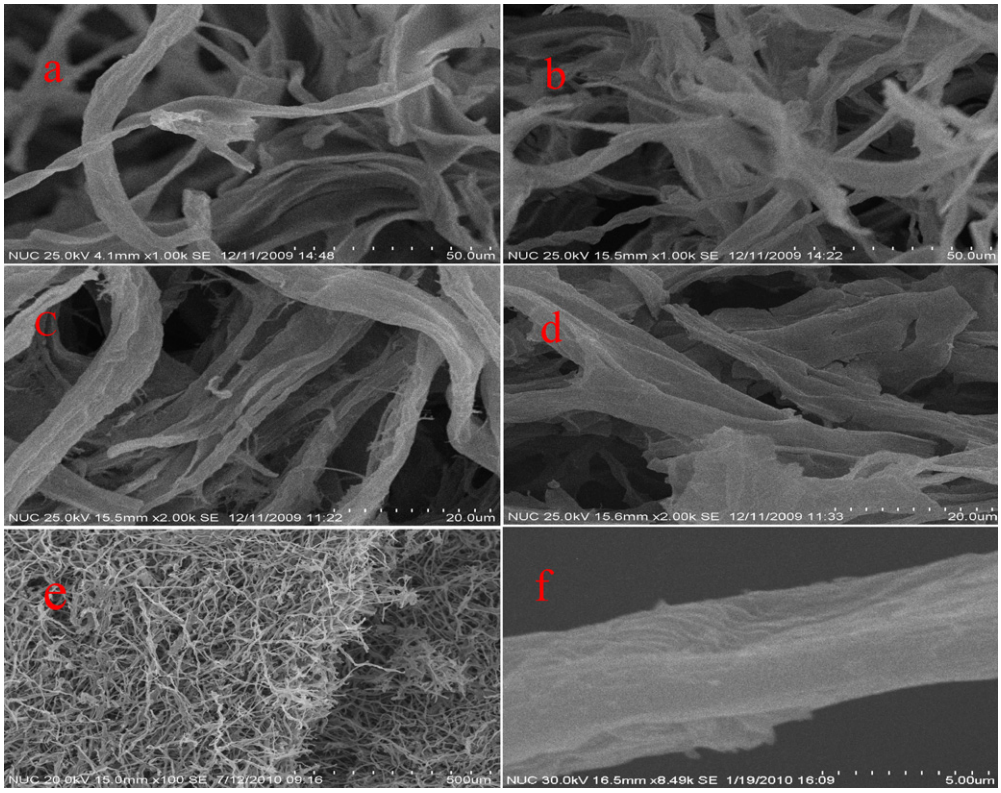

Fig. 2. SEM images of TP_{500} (a), TP_{550} (b), TP_{600} (c and e), TP_{670} (d) and an individual paper fiber (f).

formed in the samples calcined at 500 °C. Obviously, TP_{500} and TP_{600} have more surface-absorbed water and hydroxyl groups than those of P25. This can be attributed to a larger surface area of the TiO_2 paper as Ti ions are more effective in absorbing water [26]. However, further research is required to confirm the relationship between the surface area of the TiO_2 paper and the photocatalytic efficiency.

3.3. TGA investigation

Thermogravimetric analysis (TGA) was performed on the filter paper and TP_0 to evaluate the effect of the filter paper template on the formation of the TiO_2 paper and determine its removal temperature. In Fig. 5b, 5% mass less at temperature lower than 120 °C is owing to the volatility of the species (vaporization of water, elimination of the organic residue, and/or HCl) in TP_0. With an increase in the temperature there is less weight loss at 120–260 °C, corresponding to the condensation of the hydroxyl groups linked to titanium [27]. In comparison to Fig. 5a, the obvious weight loss in Fig. 5b in the temperature range 260–650 °C is attributed to the overlap of three processes, such as condensation of the hydroxyl groups linked to titanium [28], crystallization from the amorphous phase to the octahedrite crystal [29], and decomposition of the filter paper template. It can be deduced that this overlap could have an effect on the crystallization. In the DTGA curve of Fig. 5b, the downward peak at 260–350 °C is sharper than that in Fig. 5a, indicating that TP_0 has been rapidly decomposed. Meanwhile, besides

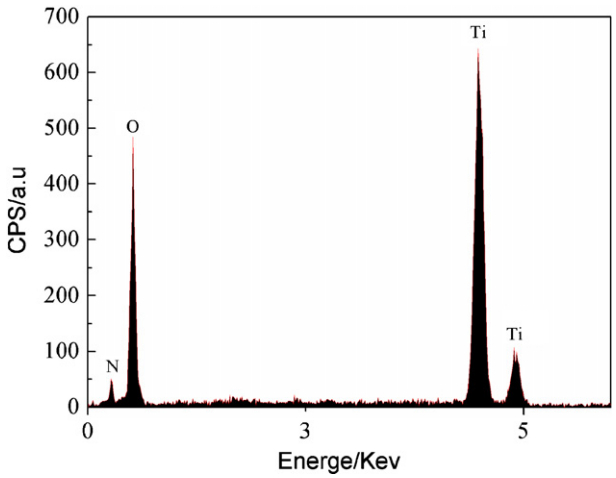

Fig. 3. EDX spectrum of TP_{600} paper.

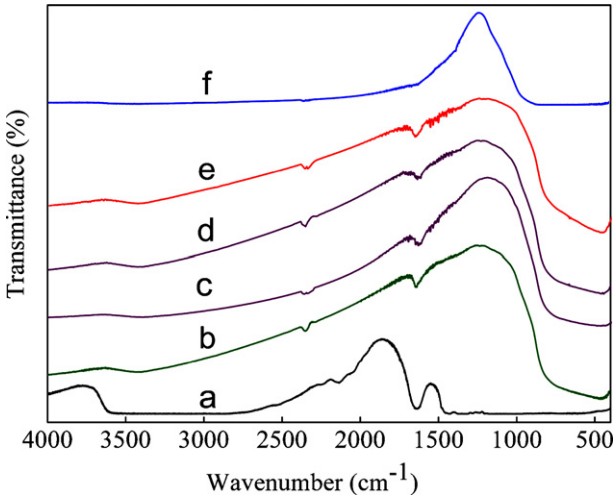

Fig. 4. FT-IR spectra of the samples obtained: TP_0 (a), TP_{500} (b), TP_{550} (c), TP_{600} (d), TP_{670} (e) and P25 (f).

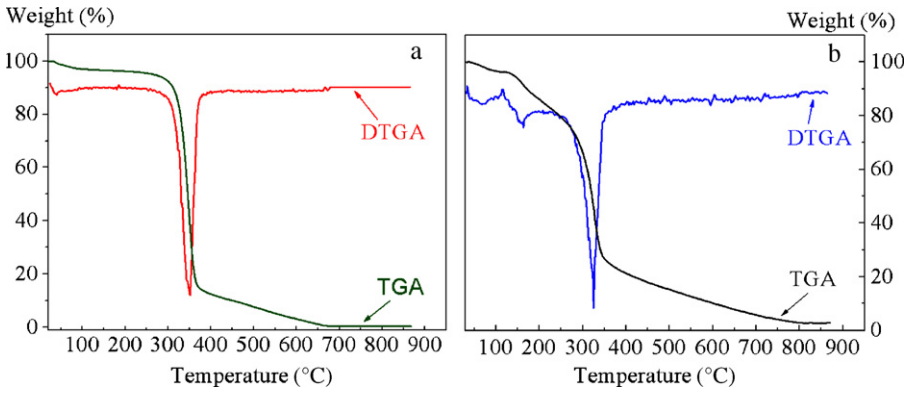

Fig. 5. TGA/DTGA curves of the filter paper (a) and TP_0 (b) at a heating rate of 1 °C/min under N_2.

the residues of the filter paper, the new materials have already started to form.

3.4. Crystal structure

The phase composition and crystallinity of the synthesized catalysts were examined by X-ray diffraction characterization. The XRD patterns of TP_{500}, TP_{550}, TP_{600}, TP_{670}, and T_{600} are illustrated in Fig. 6. Anatase (JCPDS, No. 21-1272) is the alone phase composition in TP_{500}, as evident by the diffraction peaks at the lattice parameters of 3.51 (1 0 1), 2.33 (1 1 2), 1.88 (2 0 0), 1.66 (2 1 1), 1.48 (2 0 4), 1.34 (2 2 0), and 1.26 (2 1 5). The presence of weak and board diffraction peaks also suggests the limited crystallization of TP_{500} (Fig. 6a). It can be seen that with raising calcination temperature from 500 to 670 °C, the diffraction peaks of anatase (Fig. 6a–d) become narrower and sharper. These changes indicate that the degree of crystallinity is enhanced. In the XRD spectrum of TP_{600}, the lattice parameter of 3.24 (1 1 0) (JCPDS, No. 21-1276) is identified. Thus, it is concluded that rutile have started to form around 600 °C and a certain amount of anatase transforms to rutile in TP_{600}. In Fig. 6d, it can be observed that the rutile characteristic peaks are of a greater intensity at 670 °C, particularly in the (1 1 0) lattice plane. However, anatase with high crystallinity is still the dominant phase. At the same calcination temperature of 600 °C, TP_{600} and T_{600} show the co-existence of anatase and rutile. However, the rutile peak (1 1 0) for T_{600} was higher than the anatase peak (1 0 1) in Fig. 6e, thereby indicating that rutile for T_{600} is the dominant phase. In comparison

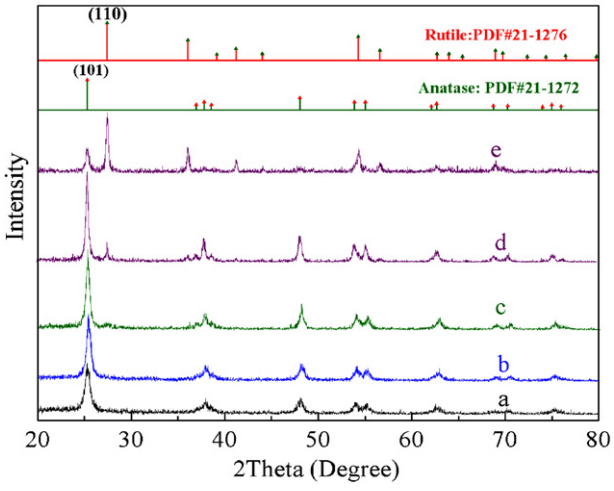

Fig. 6. XRD patterns of the synthesized samples: TP_{500} (a), TP_{550} (b), TP_{600} (c), TP_{670} (d) and T_{600} (e).

to TP_{600}, the only difference was that there is no the filter paper template in the synthesis process of T_{600}. The apparent changes in the phase content could be owing to the presence of the filter paper template.

The phase content of a sample can be calculated from the integrated intensities of the anatase and rutile peaks. If a sample contains only anatase and rutile, the weight fraction of rutile (W_R) can be calculated from Eq. (4) [30]:

$$W_R = \frac{A_R}{0.8844A_A + A_R} \quad (4)$$

where A_A represents the integrated intensity of the anatase (1 0 1) peak, and A_R represents the integrated intensity of the rutile (1 1 0) peak. The weight percentage of the anatase and rutile phase for the samples is calculated by comparing the XRD integrated intensities of (1 0 1) reflection of anatase and (1 1 0) reflection of rutile. It can be seen in Table 1 that T_{600} without using the filter paper template had a more rutile phase in comparison to TP_{600} at the same calcination temperature. The reason for the increase in the anatase–rutile transformation temperature can be attributed to three factors: (a) the pyrolysis temperature of fibers (280–500 °C as shown in Fig. 5a) and the anatase formation temperature (247–327 °C) [31] overlap. The fiber pyrolysis is endothermic reaction which can reduce the heating rate and maintain longer time in the amorphous–anatase temperature rang. This is beneficial to the anatase growth and improves the anatase stability to the high temperature; (b) the high melting point materials existing in the filter paper might restrict the anatase-rutile transformation [32]; (c) the hydroxyl groups on the surface of fiber can chelate with titanium, implying that this interaction may hinder the titanium rearrangement and raise the anatase-rutile transformation temperature [33,34].

The photocatalytic activities of the samples were tested for the photodegradation of methyl orange under UV-light irradiation. The obtained results reveal that TP_{600} shows the highest activity. It is widely accepted that the mixed phase of titania is beneficial in reducing the recombination of the photogenerated electrons and holes, resulting in an enhancement of the photocatalytic activity. It was observed that the anatase/rutile mixed phase showed a synergistic effect in enhancing the photocatalytic activity [35]. The presence of too little or too much rutile is not beneficial to the pho-

Table 1
Summary of the phase content of the samples.

Photocatalysts	Anatase (%)	Rutile (%)	A/R ratio(w/w)
TP_{500}	100	0	100/0
TP_{550}	100	0	100/0
TP_{600}	91	9	10/1
TP_{670}	81	19	10/2.46
T_{600}	27	73	10/27.04

tocatalytic activity [36]. Consequently, the optimum proportion of anatase and rutile was found to be about 10:1 in the conducted experiments.

4. Conclusions

In summary, the filter paper, a facile and cheap template, has been used in the present study to prepare the TiO_2 paper composed of interwoven TiO_2 microstrips of around 10 μm width and less than 1 μm thickness. By varying the calcination temperature, TiO_2 paper with different anatase/rutile ratios were obtained. The experimental data led to the proposal that the presence of the filter paper can improve the crystallinity and is beneficial to the formation of the TiO_2 special morphology. The above mentioned method is simple and can be extended to the preparation of other novel microstructures and their functionalized derivatives. TP_{600} with 10:1 (anatase/rutile) can be applied to air purification, water purification, and especially the decomposition of organic contamination in the aid of ultraviolet light. Some extensive researches have been done to prepare the TiO_2 microtubules using the filter paper as templates.

Acknowledgements

This research was financially supported by the Natural Science Foundation of Shanxi Province (No. 2009011099), and Returned Overseas Students Fund Projects of Shanxi Province.

References

[1] H.F. Yu, S.T. Yang, J. Alloys Compd. 492 (2010) 695.
[2] A. Fujishima, X. Zhang, D.A. Tryk, Surf. Sci. Rep. 63 (2008) 515.
[3] J. Blanco-Galvez, P. Fernandez-Ibanez, S. Malato-Rodriguez, J. Sol. Energy Eng. 129 (2007) 4.
[4] N.M. Mahmoodi, M. Arami, J. Photochem. Photobiol. A 182 (2006) 60.
[5] A.Y. Shan, T.I.M. Ghazi, S.A. Rashid, Appl. Catal. A 389 (2010) 1.
[6] Y. Cui, L. Liu, B. Li, X. Zhou, N. Xu, J. Phys. Chem. C 114 (2010) 2434.
[7] X. Chen, S.S. Mao, Chem. Rev. 107 (2007) 2891.
[8] Y. Liao, W. Que, Z. Tang, W. Wang, W. Zhao, J. Alloys Compd. 509 (2011) 1054.
[9] X. Li, T. Fan, H. Zhou, S. Chow, W. Zhang, D. Zhang, Q. Guo, H. Ogawa, Adv. Funct. Mater. 19 (2009) 45.
[10] C. Yu, J. Park, J. Solid State Chem. 183 (2010) 2268.
[11] A. Serra, E. Filippo, A. Buccolieri, M. Di Giulio, D. Manno, Sens. Actuators B 140 (2009) 563.
[12] M. Li, Y. Liu, H. Wang, H. Shen, Appl. Energy 88 (2011) 825.
[13] M. Signoretto, E. Ghedini, V. Nichele, F. Pinna, V. Crocellà, G. Cerrato, Micropor. Mesopor. Mater. 139 (2011) 189.
[14] T. Lopez, E. Ortiz, M. Alvarez, J. Navarrete, J.A. Odriozola, F. Martinez-Ortega, E.A. Páez-Mozo, P. Escobar, K.A. Espinoza, I.A. Rivero, Nanomed.: Nanotechnol. Biol. Med. 6 (2010) 777.
[15] Y.F. Tu, S.Y. Huang, J.P. Sang, X.W. Zou, J. Alloys Compd. 482 (2009) 382.
[16] J. Zhao, X. Wang, T. Sun, L. Li, J. Alloys Compd. 434 (2007) 792.
[17] M.S. Sander, M.J. Côté, W. Gu, B.M. Kile, C.P. Tripp, Adv. Mater. 16 (2004) 2052.
[18] R.E. Cochran, J.J. Shyue, N.P. Padture, Acta Mater. 55 (2007) 3007.
[19] Y. Miao, Z. Zhai, J. He, B. Li, J. Li, J. Wang, Mater. Sci. Eng. C 30 (2010) 839.
[20] T. Zhang, J. Ge, Y. Hu, Y. Yin, Nano Lett. 7 (2007) 3203.
[21] C.A. Martínez-Pérez, P.E. García-Casillas, H. Camacho-Montes, H.A. Monreal-Romero, A. Martínez-Villafañe, J. Chacón-Nava, J. Alloys Compd. 434–435 (2007) 820.
[22] X. Jiang, T. Wang, Environ. Sci. Technol. 41 (2007) 4441.
[23] S. Qiu, S.J. Kalita, Mater. Sci. Eng. A 327 (2006) 435–436.
[24] N.N. Trukhan, A.A. Panchenko, E. Roduner, M.S. Mel'guno, O.A. Kholdeeva, J. Mrowiec-Białoń, A.B. Jarzebski, Langmuir 21 (2005) 10545.
[25] T. Peng, D. Zhao, K. Dai, W. Shi, K. Hirao, J. Phys. Chem. B 109 (2005) 4947.
[26] J.C. Yu, L. Zhang, Z. Zheng, J. Zhao, Chem. Mater. 15 (2003) 2280.
[27] Y.Q. Wang, S.G. Chen, X.H. Tang, O. Palchik, A. Zaban, Y. Koltypin, A. Gedanken, J. Mater. Chem. 11 (2001) 521.
[28] J.C. Yu, L. Zhang, J. Yu, Chem. Mater. 14 (2002) 4647.
[29] A.C. Lee, R.H. Lin, C.Y. Yang, M.H. Lin, W.Y. Wang, Mater. Chem. Phys. 109 (2008) 275.
[30] H. Zhang, J.F. Banfield, J. Phys. Chem. B 104 (2000) 3481.
[31] M.M. Mohamed, W.A. Bayoumy, M. Khairy, M.A. Mousa, Micropor. Mesopor. Mater. 103 (2007) 174.
[32] B. Grzmil, M. Rabe, B. Kic, K. Lubkowski, Ind. Eng. Chem. Res. 46 (2007) 1018.
[33] X. Wu, D. Wang, S. Yang, J. Colloid Interface Sci. 222 (2000) 37.
[34] K.T. Lim, H.S. Hwang, W. Ryoo, K.P. Johnston, Langmuir 20 (2004) 2466.
[35] S. Ahmed, M.G. Rasul, W.N. Martens, R. Brown, M.A. Hashib, Desalination 261 (2010) 3.
[36] M. Yan, F. Chen, J. Zhang, M. Anpo, J. Phys. Chem. B 109 (2005) 8673.